Acid-base and Electrochemical Properties of Manganese *meso*(*ortho*- and *meta*-*N*-ethylpyridyl)porphyrins: Voltammetric and Chronocoulometric Study of Protolytic and Redox Equilibria[†]

Tin Weitner,[a,‡,*] Ivan Kos,[a] Zoran Mandić,[b] Ines Batinić-Haberle,[c] and Mladen Biruš[a]

[a]University of Zagreb, Faculty of Pharmacy and Biochemistry, Ante Kovačića 1, Zagreb 10000, Croatia

[b]University of Zagreb, Faculty of Chemical Engineering and Technology, Marulićev trg 19, Zagreb 10000, Croatia

[c]Duke University Medical Center, Department of Radiation Oncology, Durham, NC 27710, USA

Supplementary Material

[*]Corresponding author:
Tin Weitner, Ph.D.
Faculty of Pharmacy and Biochemistry
Ante Kovačića 1
Zagreb 10000
Croatia
phone: +385 1 4818 305
e-mail: tweitner@pharma.hr

[†] Dedicated to the memory of Ivan Kos, our dear friend and colleague.
[‡] Taken in part from Tin Weitner's Ph.D. thesis submitted to the University of Zagreb.

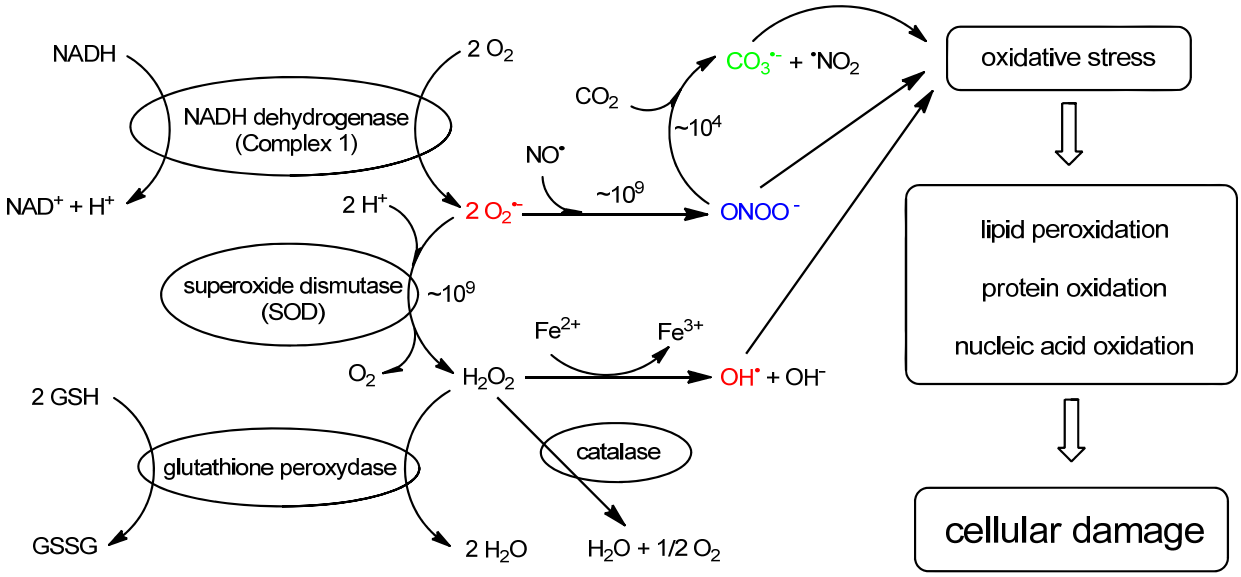

Figure S1. A schematic representation of cellular oxidative stress. The mitochondrial electron transport system is listed here as a source of $O_2^{\bullet-}$.

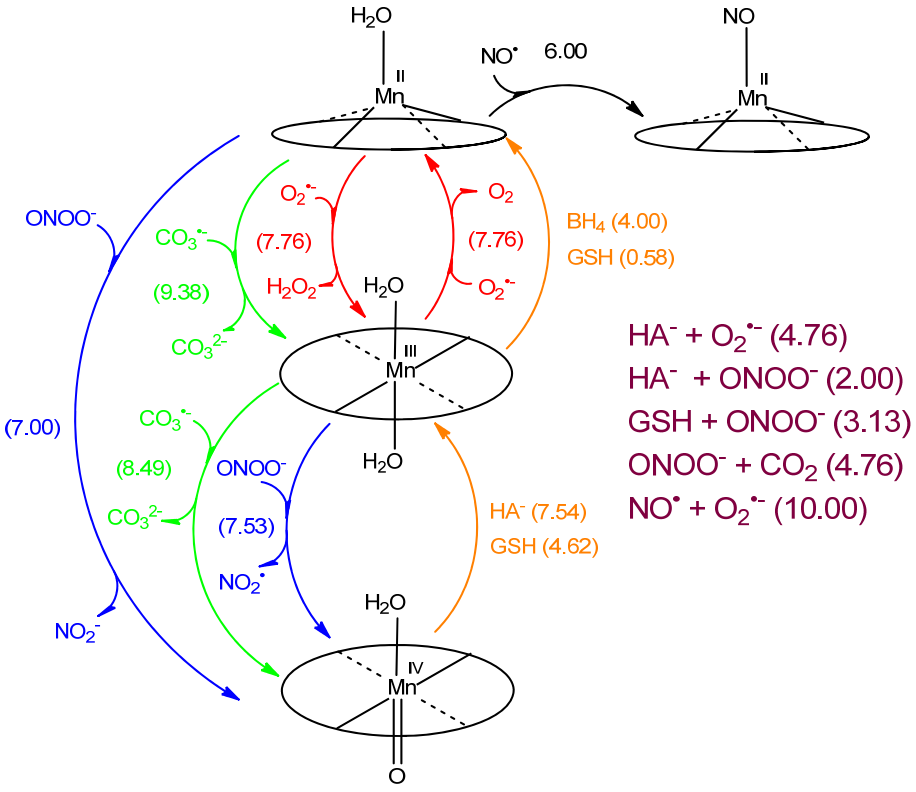

Figure S2. Reactivity scheme of manganese porphyrins in the presence of cellular reductants in aqueous solutions: HA^- ≡ monodeprotonated ascorbate, BH_4 ≡ tetrahydrobiopterin, GSH ≡ glutathione. The numbers in parentheses indicate logarithms of individual reaction rate constants, log *k*, given in M^{-1} s^{-1} (refs. 15, 23-29) Recently, a substantial amount of data indicated that MnPs react with protein thiols in the same fashion they react with GSH (refs. 30-31). Such reactions appear to be key ones in MnPs' anticancer mechanism of action. It should also be noted that the water exchange kinetics of MnPs does not limit the rate of redox kinetics under *in vivo* conditions (ref. 32).

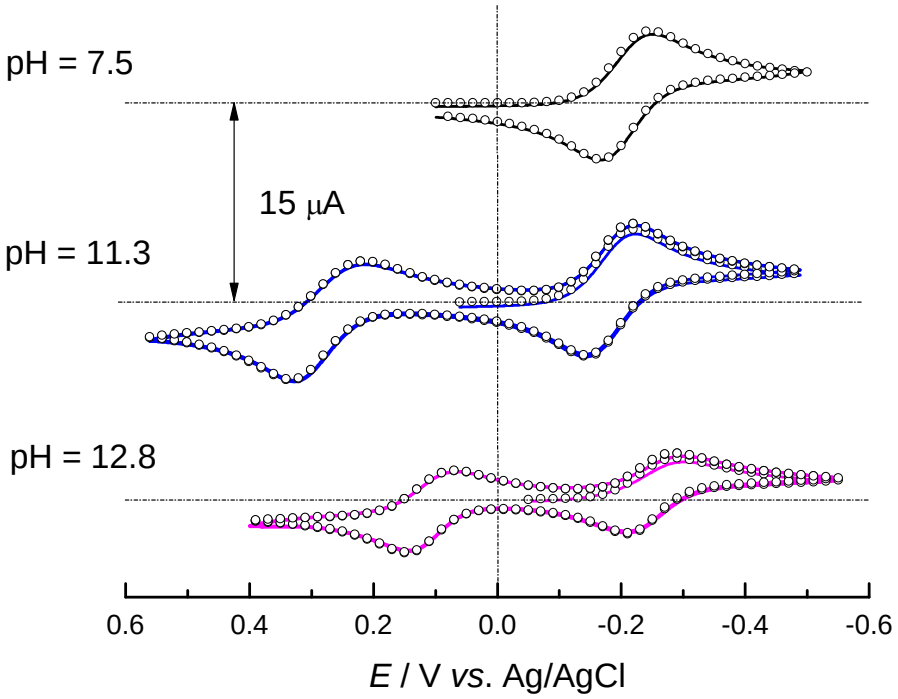

Figure S3. Dependence of cyclic voltammograms of aqueous solutions of MnTE-3-PyP on pH, v = 0.1 V s^{-1}, [NaCl] = 0.1 M, θ = 25 °C, (○) simulation in DigiElch.

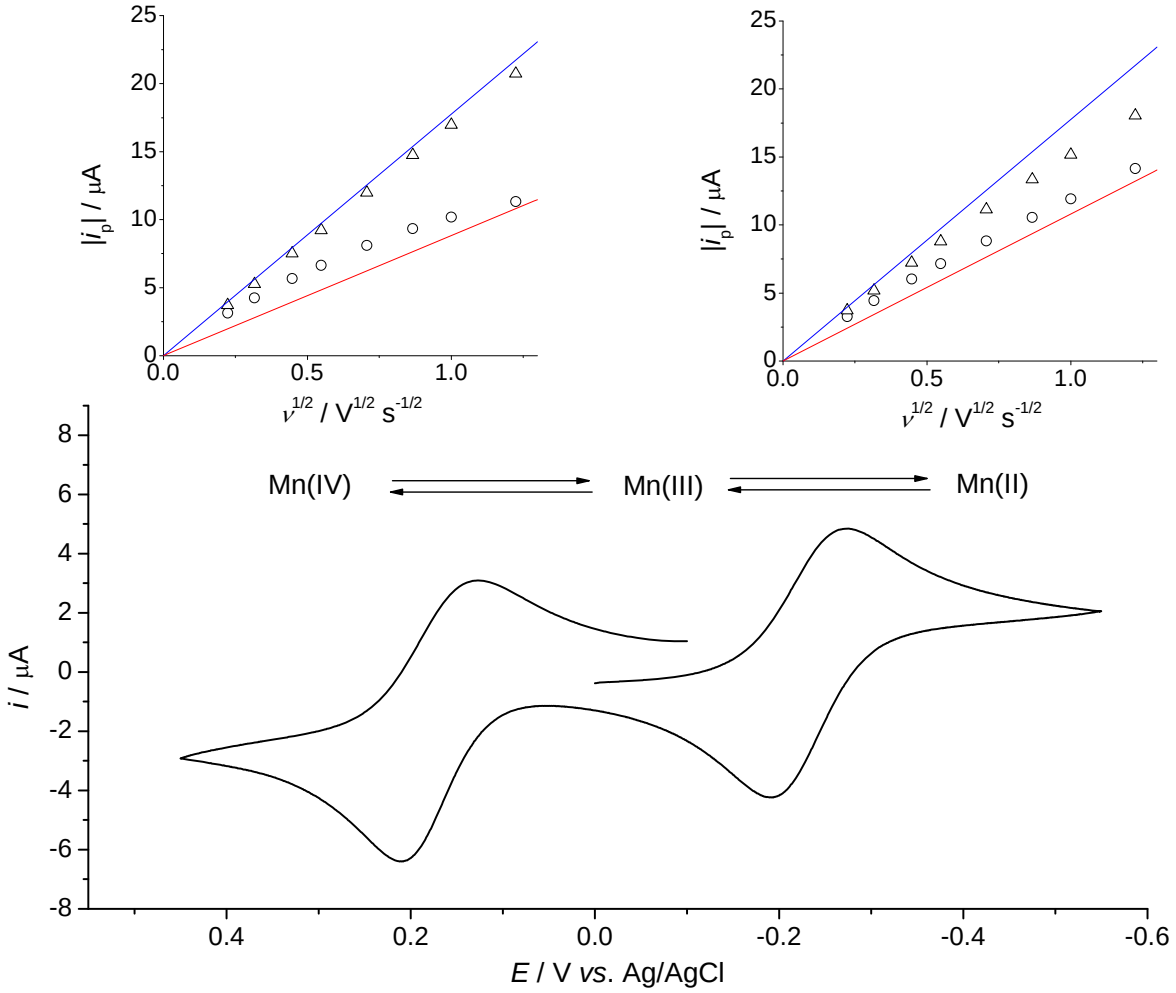

Figure S4. Cyclic voltammogram of 0.52 mM aqueous solution of MnTE-3-PyP, pH = 12.3, [Na_2HPO_4] = 50 mM, [NaCl] = 0.1 M, v = 0.1 V s^{-1}, θ = 25 °C. Inset left: Dependence of $|i_p|$ on $v^{1/2}$ for the $Mn^{IV}P/Mn^{III}P$ redox transition: i_{pc} (○), i_{pa} (Δ), Randles-Ševčik equation for the reversible electron transfer (——), peak-current equation for the irreversible electron transfer, α = 0.2 (——). Inset right: Dependence of $|i_p|$ on $v^{1/2}$ for the $Mn^{III}P/Mn^{II}P$ redox transition: i_{pc} (○), i_{pa} (Δ), Randles-Ševčik equation for the reversible electron transfer (——), peak-current equation for the irreversible electron transfer, α = 0.3 (——). The value of D_{app} obtained by chronocoulometry at the same pH (Table 2) was used for calculation.

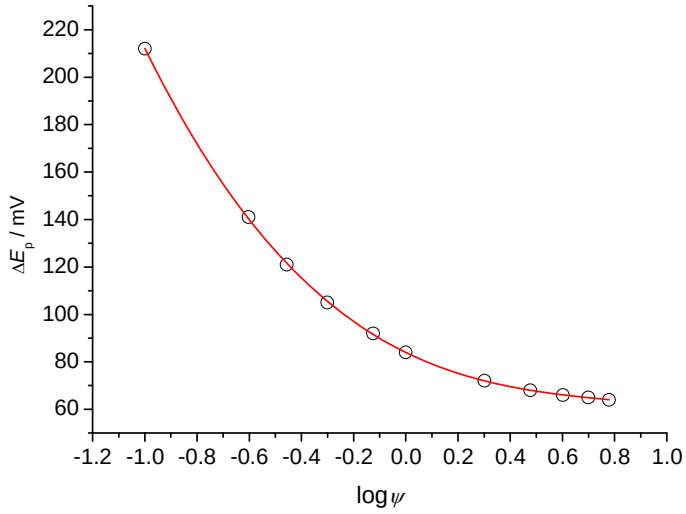

Figure S5. Dependence of ΔE_p on log ψ (○) and the polynomial model (—) given by the expression: $\Delta E_p = -21.358\ (\log \psi)^3 + 52.932\ (\log \psi)^2 - 53.849 \log \psi + 83.97$, $R^2 = 0.9999$.

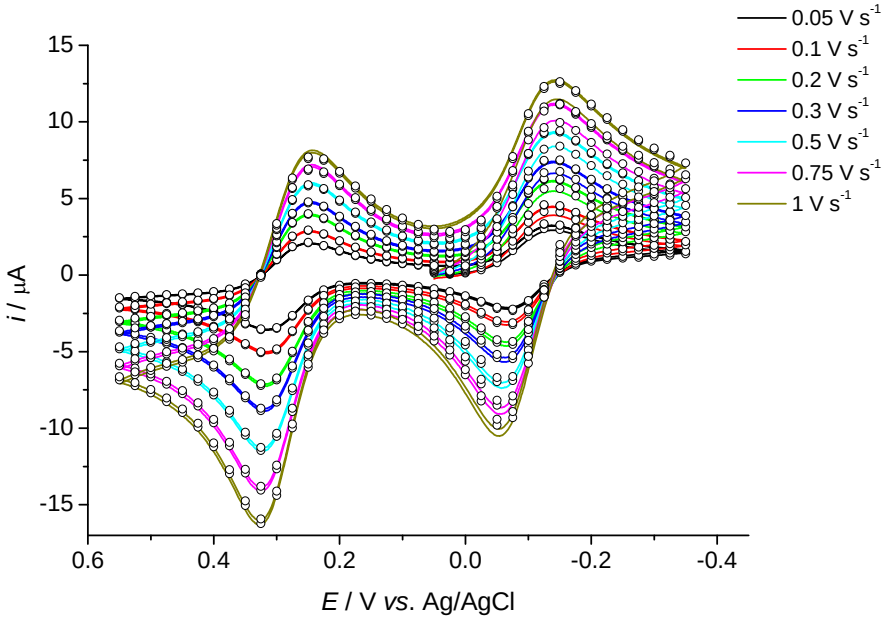

Figure S6. A typical simulation of the recorded cyclic voltammograms in DigiElch software: measured curves (–––––) and simulation (○), [MnTE-2-PyP] = 0.52 mM, pH = 11.3, [CAPS] = 50 mM, [NaCl] = 0.1 M, θ = 25 °C.

Table S7. Electrochemical parameters obtained from the recorded cyclic voltammograms of MnTE-2-PyP and MnTE-3-PyP, [NaCl] = 0.1 M, θ = 25 °C. All potentials are given *vs*. the Ag/AgCl electrode.

redox couple	MnP	pH	$E_{1/2} \pm \sigma$ / V *vs*. Ag/AgCl	$k^0_{app} \pm \sigma$ / 10^{-2} cm s^{-1}	$\alpha_{app} \pm \sigma$
$Mn^{III}P/Mn^{II}P$	MnTE-2-PyP	7.5	-0.061 ± 0.001	0.44 ± 0.04	0.433 ± 0.007
		8.4	-0.061 ± 0.001	0.48 ± 0.05	0.435 ± 0.008
		9.0	-0.062 ± 0.001	0.51 ± 0.06	0.457 ± 0.005
		9.5	-0.061 ± 0.002	0.54 ± 0.07	0.453 ± 0.008
		10.1	-0.060 ± 0.001	0.53 ± 0.04	0.453 ± 0.006
		10.5	-0.065 ± 0.001	0.55 ± 0.04	0.491 ± 0.007
		11.0	-0.090 ± 0.003	0.55 ± 0.03	0.438 ± 0.006
		11.5	-0.121 ± 0.002	0.46 ± 0.04	0.338 ± 0.003
		11.9	-0.137 ± 0.001	0.34 ± 0.03	0.385 ± 0.003
		12.5	-0.187 ± 0.003	0.30 ± 0.06	0.335 ± 0.004
		13.0	-0.238 ± 0.002	0.25 ± 0.03	0.336 ± 0.008
		13.5	-0.270 ± 0.005	0.20 ± 0.02	0.280 ± 0.006
	MnTE-3-PyP	7.5	-0.230 ± 0.002	0.22 ± 0.02	0.322 ± 0.003
		8.7	-0.229 ± 0.001	0.27 ± 0.03	0.317 ± 0.004
		9.7	-0.223 ± 0.001	0.35 ± 0.01	0.324 ± 0.005
		10.2	-0.226 ± 0.002	0.38 ± 0.03	0.334 ± 0.002
		10.8	-0.221 ± 0.002	0.40 ± 0.03	0.313 ± 0.003
		11.3	-0.223 ± 0.002	0.51 ± 0.09	0.202 ± 0.009
		12.0	-0.236 ± 0.003	0.51 ± 0.07	0.204 ± 0.010
		12.3	-0.244 ± 0.004	0.48 ± 0.03	0.164 ± 0.009
		12.8	-0.258 ± 0.002	0.42 ± 0.03	0.194 ± 0.006
		13.2	-0.285 ± 0.002	0.37 ± 0.03	0.146 ± 0.011
$Mn^{IV}P/Mn^{III}P$	MnTE-2-PyP	10.1	0.394 ± 0.003	0.14 ± 0.02	0.172 ± 0.002
		10.5	0.354 ± 0.005	0.51 ± 0.02	0.314 ± 0.004
		11.0	0.296 ± 0.004	0.47 ± 0.05	0.364 ± 0.005
		11.5	0.267 ± 0.004	0.38 ± 0.03	0.360 ± 0.004
		11.9	0.245 ± 0.005	0.38 ± 0.04	0.262 ± 0.003
		12.5	0.206 ± 0.003	0.52 ± 0.05	0.243 ± 0.003
		13.0	0.164 ± 0.003	0.45 ± 0.10	0.255 ± 0.011
		13.5	0.130 ± 0.002	0.31 ± 0.08	0.191 ± 0.009
	MnTE-3-PyP	10.2	0.459 ± 0.014	0.03 ± 0.01	0.107 ± 0.002
		10.8	0.376 ± 0.016	0.08 ± 0.01	0.135 ± 0.002
		11.3	0.301 ± 0.007	0.31 ± 0.10	0.281 ± 0.006
		12.0	0.213 ± 0.005	0.47 ± 0.05	0.468 ± 0.008
		12.3	0.178 ± 0.004	0.50 ± 0.04	0.484 ± 0.008
		12.8	0.129 ± 0.003	0.48 ± 0.04	0.487 ± 0.008
		13.2	0.088 ± 0.003	0.58 ± 0.10	0.510 ± 0.006

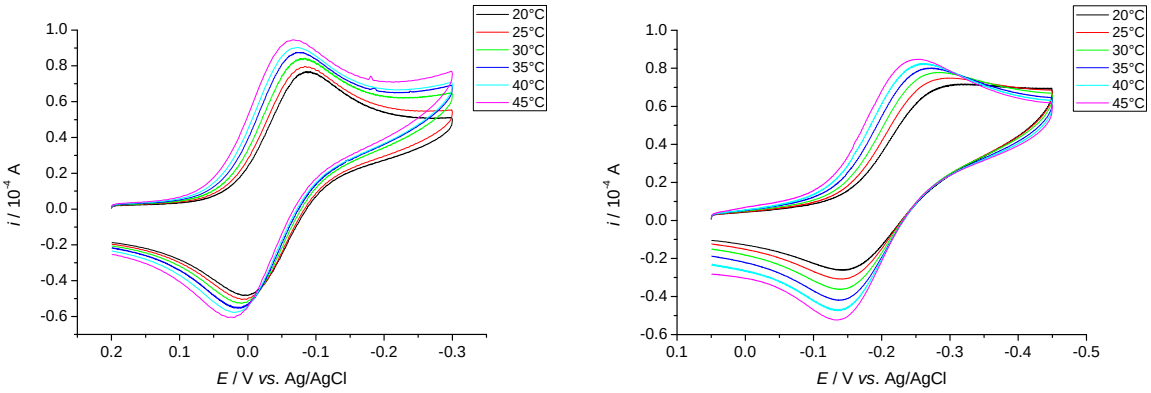

Figure S8. Cyclic voltammograms of MnPs in aqueous solution in the range from 20 °C to 45 °C, pH = 7.5, [NaH_2PO_4] = 50 mM, [NaCl] = 0.1 M, left: [MnTE-2-PyP] = 0.65 mM, right: [MnTE-3-PyP] = 0.54 mM.

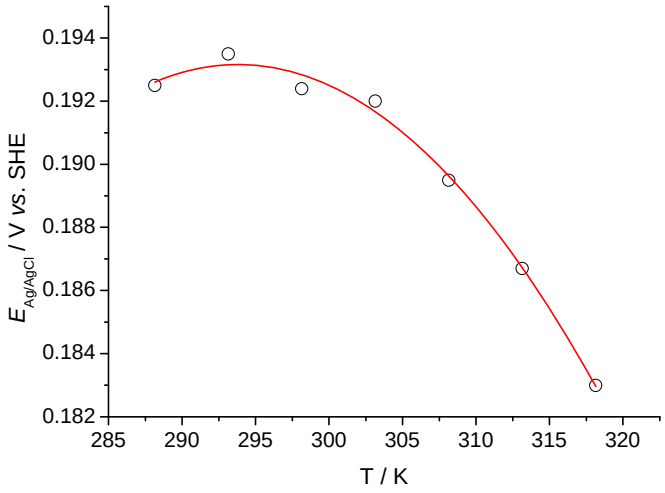

Figure S9. The temperature dependence of the potential of the Ag/AgCl electrode *vs*. SHE (○) in aqueous solution in the range from 15 °C to 50 °C and the polynomial model (—) given by the expression: $E_{Ag/AgCl}$ *vs*. SHE = – 1.72381 × 10^{-5} T^2 + 0.01013 T – 1.29508, R^2 = 0.9948, pH = 7.5, [NaH_2PO_4] = 50 mM, [NaCl] = 0.1 M.

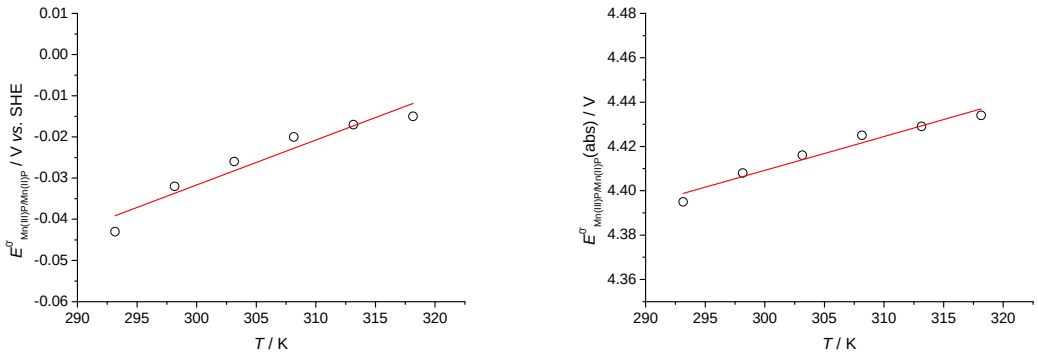

Figure S10. The temperature dependence of the formal reduction potential ($E^{0'}$ *vs*. SHE) and the absolute reduction potential ($E^{0'}$(abs)) of $Mn^{III}P/Mn^{II}P$ redox couple of MnTE-3-PyP: [MnTE-3-PyP] = 0.54 mM, pH = 7.5, [NaH_2PO_4] = 50 mM, [NaCl] = 0.1 M.

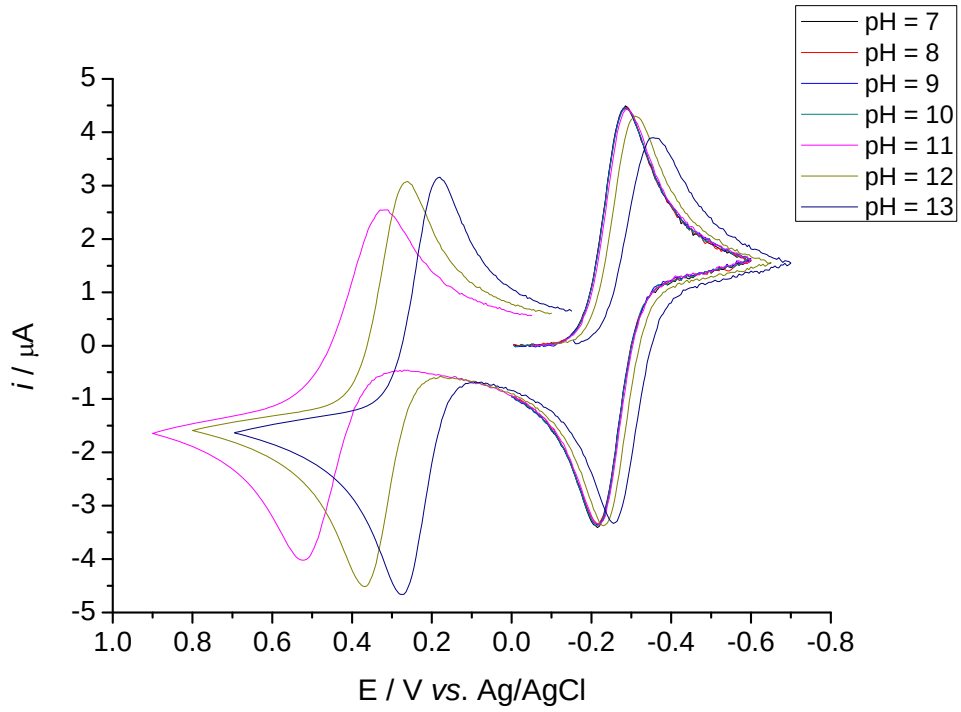

Figure S11. Simulation of the electrochemical behaviour of a 0.5 mM solution of MnTE-3-PyP in the range of pH values form 7 to 13.

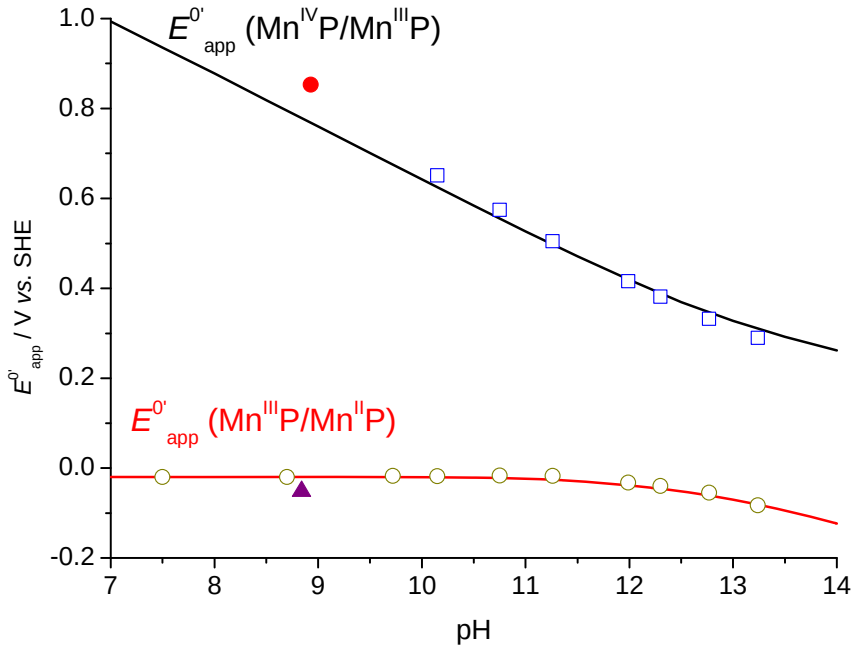

Figure S12. Comparison of the pH-dependent apparent formal reduction potentials, $E^{0'}_{app.}$, of the $Mn^{III}P/Mn^{II}P$ and $Mn^{IV}P/Mn^{III}P$ redox couples of MnTE-3-PyP simulated by eqs. (5) and (8) with various experimental values: (●) oxidation of $Mn^{III}P$ with octacyanomolybdate (ref. 35), (□) cyclic voltammetry of the $Mn^{IV}P/Mn^{III}P$ redox couple (Table S7), (▲) reduction of $Mn^{III}P$ with ascorbate (ref. 35), and (○) cyclic voltammetry of the $Mn^{III}P/Mn^{II}P$ redox couple (Table S7).

Table S13. Electrochemical parameters for the reduction of the experimentally accessible species of MnTnBu-2-PyP in aqueous solutions, [NaCl] = 0.1 M, θ = 25 °C. Values of the deprotonation constants were taken from ref. 50: pK'_{a1} = 10.6, pK_{a1} = 10.3, pK_{a2} = 11.2, pK''_{a3} = 10.3. As previously in Figures 7, 8, S11 and S12, the experimentally unavailable deprotonation constants were taken to be at least one pH unit beyond the studied pH range, i.e. pK'_{a2} = 14, pK_{a3} = 14, pK_{a4} = 15, pK''_{a1} = 5, pK''_{a2} = 6, pK''_{a4} = 14.

MnP	couple	index	$E_i^{0'}$ / V *vs.* SHE
MnTnBu-2-PyP	$Mn^{III}P/Mn^{II}P$	1	0.203
		2	0.185
		3	≤ 0.020
	$Mn^{IV}P/Mn^{III}P$	5	≥ 0.836
		6	0.528
		7	≤ 0.309

Table S14. Thermodynamic parameters for the reactivity of MnTE-2-PyP and MnTE-3-PyP with $ONOO^-$ in a neutral aqueous medium. All potentials are given in V *vs*. SHE.

MnP	MnTE-2-PyP	MnTE-3-PyP
$E^{0'}(Mn^{IV}P/Mn^{III}P)$ / V (eq. 14, pH = 7)	0.980	0.993
$E^{0'}(Mn^{III}P/Mn^{II}P)$ / V (eq. 11, pH = 7)	0.145	-0.020
$E^{0'}(Mn^{IV}P/Mn^{II}P)^*$ / V (pH = 7)	0.563	0.487
$E^{0'}(ONOO^-/NO_2^{\bullet})$ / V (ref. 79)	1.600	1.600
$E^{0'}(ONOO^-/NO_2^-)$ / V (ref. 79)	1.300	1.300
EMF $(1e^-)^{**}$ / V	0.620	0.607
EMF $(2e^-)^{**}$ / V	0.738	0.814

* $E^{0'}(Mn^{IV}P/Mn^{II}P) = (E^{0'}(Mn^{III}P/Mn^{II}P) + E^{0'}(Mn^{IV}P/Mn^{III}P))/2$.

** $EMF = E_c - E_a$ for single-electron and two-electron reduction of $ONOO^-$, *EMF* $(1e^-)$ and *EMF* $(2e^-)$, where the values of E_c are the formal potentials $E^{0'}(ONOO^-/NO_2^{\bullet})$ and $E^{0'}(ONOO^-/NO_2^-)$, respectively, whereas the values of E_a are the formal potentials $E^{0'}(Mn^{IV}P/Mn^{III}P)$ and $E^{0'}(Mn^{IV}P/Mn^{II}P)$, respectively.